

NGC 5824: a luminous outer halo globular cluster with an intrinsic abundance spread

G. S. Da Costa,¹ E. V. Held,² and I. Saviane³

¹*Research School of Astronomy and Astrophysics, Australian National University, Canberra, ACT 0200, Australia*

²*INAF, Osservatorio Astronomico di Padova, vicolo Osservatorio 5, 35122 Padova, Italy*

³*European Southern Observatory, Alonso de Cordova 3107, Santiago, Chile*

12 September 2018

ABSTRACT

We present a detailed study of the strengths of the calcium triplet absorption lines in the spectra of a large sample of red giant members of the luminous outer Galactic halo globular cluster NGC 5824. The spectra were obtained with the FORS2 and GMOS-S multi-object spectrographs at the VLT and the Gemini-S telescope, respectively. By comparing the line strengths of the NGC 5824 stars with those for red giants in clusters with well established abundances, we conclude that there is an intrinsic abundance dispersion in NGC 5824 characterized by an inter-quartile range in $[\text{Fe}/\text{H}]$ of 0.10 dex and a total range of ~ 0.3 dex. As for ω Cen and M22, the abundance distribution shows a steep rise on the metal-poor side and a shallower decline on the metal-rich side. There is also some indication that the distribution is not unimodal with perhaps 3 distinct abundance groupings present. NGC 5824 has a further unusual characteristic: the outer surface density profile shows no signs of a tidal cutoff. Instead the profile has a power-law distribution with cluster stars detected to a radius exceeding 400 pc. We postulate that NGC 5824 may be the remnant nuclear star cluster of a now disrupted dwarf galaxy accreted during the formation of the Galaxy’s halo. We further speculate that the presence of an intrinsic $[\text{Fe}/\text{H}]$ spread is the characteristic that distinguishes former nuclear star clusters from other globular clusters.

Key words: globular clusters: general; globular clusters: individual (NGC 5824); stars: abundances; stars: Population II

1 INTRODUCTION

On the basis of many detailed spectroscopic and photometric studies carried out over more than a decade, we can now assert with some conviction that most, if not all, of the globular clusters associated with the Milky Way galaxy are not the simple stellar populations they were once considered to be. The evidence to support this assertion can be found in, for example, the sodium-oxygen abundance anti-correlation that pervades the stars in essentially all Galactic globular clusters (see the recent review of Gratton et al. 2012). While the exact nature of the “polluters” that give rise to the chemical anomalies remains uncertain, it is clear that the production of the anomalies is intimately connected to the formation process of the cluster, and not to any process involving the current generation of cluster stars.

Nevertheless, despite the ubiquity of the abundance inhomogeneities involving the light elements C, N, O, Na, Mg and Al, it remains the case that most globular clusters are chemically homogeneous with respect to the heavier

elements such as Fe and Ca (e.g., Carretta et al. 2010b), elements whose nucleosynthesis lies with supernovae. The classic exception to this general situation is the stellar system ω Cen, which has been known to have an unusual stellar population for almost four decades. Specifically, the stars in ω Cen possess a large range in iron abundance together with distinct element-to-iron abundance ratios (e.g., Johnson & Pilachowski 2010; Marino et al. 2012, and the references therein). These unusual characteristics have led to the suggestion that the stellar system ω Cen is “special”, in that it is the nuclear remnant of a now disrupted dwarf galaxy (e.g., Freeman 1993). Chemical evolution models of such systems have been moderately successful in reproducing the observed properties of the cluster (e.g., Romano et al. 2007, 2010; Marcolini et al. 2007) and dynamical models of the tidal disruption process (e.g., Bekki & Freeman 2003) have also shown that plausible scenarios exist in which the nuclear remnant can end up in an orbit similar to the tightly bound and retrograde orbit

of the current cluster. The strongest evidence in support of this hypothesis for the origin of ω Cen, however, comes from the recent discovery of field stars that show unusual chemical abundance ratios similar to cluster member stars (Wylie de Boer et al. 2010; Majewski et al. 2012).

It is now recognised, however, that ω Cen is not the only Galactic globular cluster with an internal [Fe/H] abundance spread, although it remains the object with the largest star-to-star [Fe/H] range. For example, the nuclear star cluster of the Sagittarius dwarf galaxy, M54, was first suggested to have an intrinsic abundance spread, $\sigma_{int}([\text{Fe}/\text{H}])$, of ~ 0.16 dex by Sarajedini & Layden (1995) on the basis of the intrinsic colour width of the cluster red giant branch. Subsequent analyses based on intermediate- and high-resolution spectra of a significant number of M54 red giants have confirmed the existence of this intrinsic spread, yielding $\sigma_{int}([\text{Fe}/\text{H}]) \approx 0.19$ dex (e.g., Carretta et al. 2010a, and the references therein). The Sgr dwarf is currently under going tidal disruption, which when complete will leave M54 as a member of the Galactic halo globular cluster population, and its status as a nuclear star cluster of a dwarf galaxy will then no longer be obvious.

A third cluster with an intrinsic range in [Fe/H] abundance is M22. Da Costa et al. (2009) used intermediate-resolution spectra at the Ca II triplet of 41 member stars to demonstrate that there is a broad [Fe/H] abundance distribution in this cluster qualitatively similar (but on a smaller scale) to that for ω Cen. The abundance distribution reveals the presence of at least two components and is characterised by an interquartile range in [Fe/H] of 0.24 dex (Da Costa et al. 2009). Similar results have been found from the high dispersion spectroscopic analyses of Marino et al. (2009, 2011). These data show the presence of two populations in the cluster, one of which is enhanced in *s*-process elements and Fe relative to the other (Marino et al. 2009, 2011, see also Roederer et al. (2011)). With $M_V = -8.5$ (Harris 1996)¹, M22 is not especially luminous (as M54 and ω Cen are) and it is kinematically a typical inner-halo globular cluster (Dinescu et al. 1999). It is not known to be associated with any dwarf galaxy remnant or stellar stream.

Three other Galactic globular clusters also show significant (i.e., $\sigma_{int}[\text{Fe}/\text{H}] \gtrsim 0.05$ dex) intrinsic [Fe/H] ranges. These are the metal-rich bulge cluster Terzan 5 (Ferraro et al. 2009) and the intermediate metallicity clusters NGC 1851 (Carretta et al. 2011) and NGC 3201 (Simmerer et al. 2013). Terzan 5 shows two distinct stellar populations that differ by ~ 0.5 dex in [Fe/H] and which also have different α -element to iron abundance ratios, suggesting a complex enrichment history (Origlia et al. 2011). NGC 1851, on the other hand, shows a relatively small intrinsic iron abundance dispersion characterised by $\sigma_{int}([\text{Fe}/\text{H}]) \approx 0.07$ dex (Carretta et al. 2011). There is, however, a tendency for the more iron-rich stars to have also higher abundances of the *s*-process element Ba (Carretta et al. 2011), a situation reminiscent of the two (Fe, *s*-process) groups in M22. NGC 1851 has a number of other abundance and photometric peculiarities (e.g.,

Milone et al. 2008; Yong et al. 2009; Carretta et al. 2011, 2012). Potential scenarios to explain the observations include the possibility that the current cluster is the product of the merger of two separate globular clusters within a (now disrupted) parent dwarf galaxy (Carretta et al. 2011, and the references therein). The presence of an extensive stellar halo around NGC 1851 (Olszewski et al. 2009; Carballo-Bello et al. 2012) may be a remnant of the disrupted dwarf, although the recent results of Sollima et al. (2012) show that the situation is complex, with the stellar halo apparently containing more than one component. As regards NGC 3201, which has a highly retrograde orbit and a luminosity $M_V = -7.45$ (Harris 1996), somewhat fainter than that of NGC 1851 ($M_V = -8.3$), the high dispersion spectroscopic analysis of Simmerer et al. (2013) for 24 member red giants revealed a total [Fe/H] abundance range of ~ 0.4 dex with $\sigma_{int}([\text{Fe}/\text{H}]) \approx 0.1$ dex. However, more recently, Muñoz et al. (2013) did not find any strong evidence for a substantial abundance range in this cluster from their high dispersion study of 8 NGC 3201 red giants: the dispersion in the [Fe/H] values was only 0.04 dex and the range in the observed abundances was 0.12 dex. Similarly, Carretta et al. (2009) and Saviane et al. (2012) also did not find any significant evidence for an abundance range in this cluster.

In the above discussion we have left aside clusters such as M15, which shows an intrinsic spread in neutron-capture elements, particularly the *r*-process element Eu, but not in [Fe/H] (Sobeck et al. 2011, and references therein). Indeed Yong et al. (2013) propose that the Galactic globular clusters can be grouped into three classes: (i) those that exhibit abundance variations in the light elements only; (ii) those which in addition to the light element variations show a range in the abundances of neutron-capture elements; and, (iii) those which also possess an intrinsic dispersion in the Fe-peak element abundances. The one exception to this scheme is the luminous extreme outer halo globular cluster NGC 2419, which appears to be a very different stellar system as regards its elemental abundances. Mucciarelli et al. (2012, and the references therein) show that the red giants in this cluster have very similar [Fe/H], [Ca/Fe] and [Ti/Fe] abundance and abundance ratios while at the same time possessing large anti-correlated variations in Mg and K abundances. The origin of these abundance anomalies is not easily explained (Mucciarelli et al. 2012).

In a recent paper Saviane et al. (2012) reported that the relatively unstudied cluster NGC 5824 could be a further Galactic globular cluster with an intrinsic [Fe/H] abundance range. This object is a metal-poor globular cluster that lies 32 kpc from the Sun and 26 kpc the Galactic Center in the outer halo (Harris 1996). With $M_V = -8.9$ it is a relatively luminous system: for the globular clusters further from the Galactic Center than M54 (i.e., $R_{GC} \gtrsim 20$ kpc), only NGC 2419 is more luminous (Harris 1996). NGC 5824 is also highly centrally concentrated ($c = 2.0$) with a small core-radius of 0.6 pc (Harris 1996). The cluster is of further interest because of its possible association with the Cetus Polar Stream (Newberg et al. 2009). The Cetus Polar Stream is low luminosity metal-poor stellar stream in the south Galactic gap characterised by blue horizontal branch stars (Newberg et al. 2009; Koposov et al. 2012). Newberg et al. (2009) did not observe the stream in

¹ Data values used are those from the latest version of the Harris (1996) catalogue available at <http://physwww.physics.mcmaster.ca/~harris/mwgc.dat>.

the vicinity of NGC 5824, which is in fact in the opposite Galactic hemisphere, but noted that the cluster has a location, distance, and radial velocity consistent with the predictions of the best-fit orbit to their Cetus Polar Stream data (Newberg et al. 2009). The metallicity is also consistent with that of the stream stars (Newberg et al. 2009).

NGC 5824 was included in the Saviane et al. (2012) study because the only previous metallicity estimate was based on an integrated light spectrum. Intermediate-resolution spectra at the Ca II triplet were obtained for 17 red giant branch members. The line strength data showed a dispersion that was notably larger than that expected from the measurement errors alone, leading to the suggestion of the presence of an internal abundance spread characterised by $\sigma_{int}([\text{Fe}/\text{H}]) \approx 0.12$ dex (Saviane et al. 2012). As noted by Saviane et al. (2012), NGC 5824 was the only cluster besides M22 and M54 in the sample of 20 program and 8 ‘standard’ clusters studied to show a spread in line-strengths in excess of that expected from the errors.

Given the relatively small numbers of Galactic globular clusters with intrinsic $[\text{Fe}/\text{H}]$ distributions, it is important to verify the Saviane et al. (2012) results. We present here the outcome of an intermediate-resolution spectroscopic study of a much larger sample of NGC 5824 red giants than that presented in Saviane et al. (2012). The observations and data analysis techniques are discussed in the following section, while in §3 we pay careful attention to the cluster membership status for the stars in the observed sample. The results for the final set of cluster red giant probable members are presented in §4 and are discussed in a broader context in the final section.

2 OBSERVATIONS AND REDUCTIONS

2.1 Sample Selection

Observing time to follow-up the possibility of an intrinsic $[\text{Fe}/\text{H}]$ spread in NGC 5824 was allocated for intermediate-resolution spectroscopy of candidate red giant members on both the VLT with the FORS2 multi-object spectrograph, and on the Gemini-S telescope with the GMOS-S multi-object spectrograph. The targets for the GMOS-S observations were chosen from the photometry derived from the CCD images of the cluster obtained as pre-imaging for the FORS2 observations discussed in Saviane et al. (2012). In this case the images were centered on the cluster. For the new FORS2 observations, a further set of pre-images (30 s exposures in V and I) was obtained that covers a larger area around the cluster. In both cases the list of potential targets was restricted to those stars that lie relatively close to the cluster red giant branch (RGB) in the colour-magnitude diagrams derived from the imaging data. The selected stars were also chosen to cover a magnitude range from the vicinity of the RGB tip to approximately 0.5 mag brighter than the horizontal branch magnitude.

The photometry derived from the new FORS2 pre-imaging, which was obtained over a number of nights and under different seeing conditions, was subsequently brought on to a single system using stars in the field-to-field overlap regions, and calibrated to the standard V , I system using stars whose standard magnitudes are available in the photo-

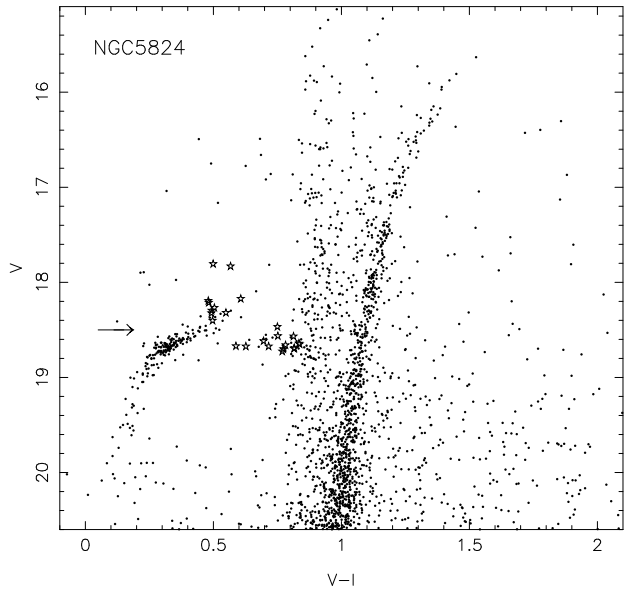


Figure 1. Color-magnitude diagram for NGC 5824 from the FORS2 pre-imaging data. Only stars outside $50''$ from the cluster center are shown. The maximum radial distance is $8.1'$. The horizontal arrow indicates the adopted value of $V(HB)$ for the cluster. Known RR Lyrae variables in the cluster which occur in the FORS2 photometry list are plotted as open-star symbols.

metric standard star fields database maintained by Stetson². The stars observed with GMOS-S are included in this calibrated photometry set.

In Fig. 1 we show the final calibrated colour-magnitude diagram (CMD) for NGC 5824 from the FORS2 pre-imaging. The conventional definition of $V(HB)$, the mean magnitude of the horizontal branch, for clusters like NGC 5824 that have a strong blue horizontal branch (HB) population, is the mean magnitude of the HB stars at the blue edge of the RR Lyrae instability gap. The blue edge lies at $(B - V)_0 \approx 0.22$ in metal-poor globular clusters (e.g., Sandage 2006) which, allowing for the NGC 5824 reddening of $E(B - V) = 0.13$ (Harris 1996), corresponds to $(V - I) \approx 0.47$ mag. Our CMD then suggests for NGC 5824 $V(HB) = 18.50$ with an uncertainty of ± 0.03 mag. This value is in good agreement with the value $V(HB) = 18.45$ tabulated by Harris (1996), which is derived from the CMD study of Brocato et al. (1996). It is also consistent with NGC 5824 CMD derived from *HST* WFPC2 photometry in Piotto et al. (2002). Also shown in the figure is the photometry from the pre-imaging data for 24 of the 27 NGC 5824 variable stars (all candidate RR Lyrae variables) listed in the on-line version of the Globular Cluster Variable Star Catalogue³ (Clement et al. 2001) that we were able to unambiguously identify via a position match. It is likely that the search for variables in this cluster is not complete.

² <http://www3.cadc-ccda.hia-ihp.nrc-cnrc.gc.ca/community/STETSON/standards/>

³ <http://www.astro.utoronto.ca/~cclement/read.html>

2.2 Spectroscopic Observations

2.2.1 VLT

The spectroscopic observations of the candidate NGC 5824 red giants defined from the pre-imaging data were carried out in Service Mode with the FORS2 instrument (Appenzeller et al. 1998) at the Cassegrain focus of VLT1/UT1-Antu under ESO program 087.D-0465. The instrumental setup employed was identical to that used in Saviane et al. (2012): MOS-mode with 1'' slit widths and with the 1028z+29 grism plus the OG590+32 order-blocking filter providing a maximum spectral coverage of $\sim\lambda 7700\text{--}9500\text{\AA}$ which includes the Ca II triplet feature. The MOS-mode uses 19 moveable slitlets of 20'' length that are placed on the target stars. A total of 14 MOS-configurations were observed over seven nights in the period 9 May 2011 to 27 June 2011. Each observation consisted of a pair of 480 s integrations. One of the MOS configurations observed was deliberately chosen to be identical to that observed in Saviane et al. (2012). Bias frame, arc lamp and flat-field exposures were also obtained in the morning following each observing night as part of the standard calibration procedures.

2.2.2 Gemini South

Observations of candidate NGC 5824 red giants were also carried out in Queue-Scheduled mode on the Gemini-S telescope under program GS-2011A-Q-47 using the GMOS-S multi-object spectrograph. The spectrograph was configured with the R831 grating and a RG610 filter and set to a central wavelength of 8600Å. Four masks were observed on 6 May 2011 with a fifth observed on 13 May 2011. For both observations the seeing was $\sim 1''$ with relatively clear skies, consistent with the requested conditions. Each mask used a slit width of 1'' and a slit length 10'' to allow adequate subtraction of the bright night-sky emission line features. A total of 76 candidate red giant branch stars (plus 3 acquisition stars per mask) were allocated across the 5 masks. One star was common to four masks, two were common to three masks and one common to two masks. The sample also included NGC 5824 red giants originally observed in Saviane et al. (2012) to ensure line strength measures from the GMOS-S spectra could be placed on the same system as that of the FORS2 spectra.

The observation of each mask consisted of a 1200 s integration at the central wavelength of 8600Å followed by a second 1200 s integration at a central wavelength of 8550Å, with each observation followed or preceded by a flat field integration at the corresponding central wavelength. The observations with different central wavelengths allow for the possibility of a Ca II triplet feature falling on the gaps between the three GMOS-S CCD detectors. Arc lamp exposures for each mask were obtained as part of the routine baseline calibration procedures.

2.3 Data Reduction

2.3.1 FORS2

The FORS2 spectral data were reduced using version 4.6.3 of the FORS2 pipeline (Izzo & Larsen 2008) in an identi-

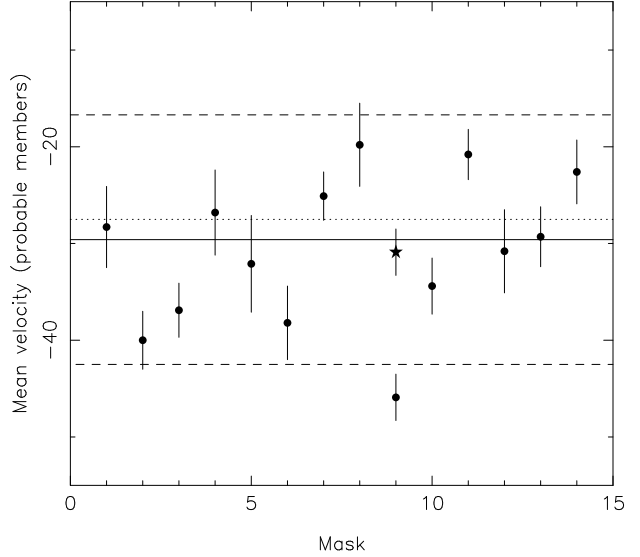


Figure 2. The mean heliocentric velocity for NGC 5824 probable members is shown as a filled circle for each of the fourteen masks observed with FORS2. The error bar associated with each point is the standard deviation of the mean. The dotted line is the NGC 5824 cluster velocity given in Harris (1996), while the solid line is the average of the mask mean velocities, excluding mask 9. The dashed lines are $\pm 2\sigma$ about this average value. The star symbol shows the location of the mean velocity for mask 9 after an adjustment of $+15 \text{ km s}^{-1}$.

cal manner to that described in Saviane et al. (2012). The two exposures per mask were average-combined after the pipeline processing and the final reduced spectra have a resolution of $\sim 3.5\text{\AA}$ at $\lambda 8600\text{\AA}$ and a scale of 0.82 \AA per pixel. A total of 233 useable spectra of 172 stars resulted.

The radial velocities for the stars in each of the 14 FORS2 masks were measured using the three lines ($\lambda\lambda 8498, 8542$ and 8662\AA) of the Ca II triplet and the IRAF package RVIDLINES following an identical process to that adopted in Saviane et al. (2012). In Fig. 2 we show the mean heliocentric velocity for the probable NGC 5824 members in each mask. In general there is reasonable agreement between these mean mask velocities and the Harris (1996) catalogue velocity ($-27.5 \pm 1.5 \text{ km s}^{-1}$) for the cluster. The one exception is mask 9 where the mean velocity of the probable members is $\sim 15 \text{ km s}^{-1}$ lower than the mean velocity for the other 13 masks. Consequently, we have adjusted the velocities for the stars observed in this mask by $+15 \text{ km s}^{-1}$ to place them in accord with the other FORS2 velocities. We note in particular that unlike the earlier NGC 5824 velocities discussed in Saviane et al. (2012), we see no disagreement between the FORS2 velocities derived here and the Harris (1996) catalogue velocity for the cluster.

2.3.2 GMOS-S

The CCD detectors in GMOS-S at the time of the observations fringe badly at wavelengths beyond $\sim 7000\text{\AA}$. It is the ability to deal with this large amplitude fringing that ultimately sets the signal-to-noise of the reduced spectra rather than the actual signal. The data frames for each mask were reduced following example IRAF Gemini package scripts, modified during the course of the process to achieve as

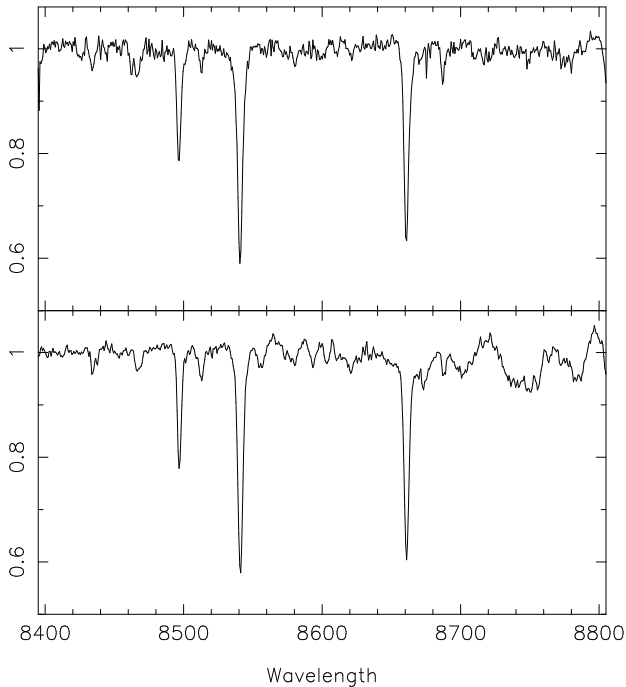


Figure 3. Examples of fully reduced GMOS-S spectra from the observations of Mask 1 at a central wavelength of 8600Å. The upper panel shows the spectrum of star 42008180 ($V=16.51$) in which the fringing has been substantially removed, while the lower panel shows the spectrum of star 42012704 ($V=16.19$) for which significant residual fringing remains.

best a reduction in the fringe amplitude as possible. In this process the frames with the different central wavelengths, which have the Ca II triplet features at different locations on the detectors and which are thus subject to different fringing, were kept separate. The final wavelength-calibrated, sky-subtracted spectra have a resolution of $\sim 3.5\text{\AA}$ and a (binned) pixel-scale of 0.68\AA per pixel. Examples of GMOS-S spectra where the fringing compensation has worked well, and where it has not, are shown in Fig. 3.

As for the FORS2 spectra, initial radial velocity estimates for each of the stars observed with GMOS-S were determined by measuring with RVIDLINES the Ca II triplet line centers on the reduced spectra. The velocities from the $\lambda 8600\text{\AA}$ and $\lambda 8550\text{\AA}$ central wavelength observations for each star were then averaged. Since the arc lamp exposures for each mask and central wavelength setting were carried out during daylight hours (and in one case on a different day) the zero point of the velocity scale for each mask is not necessarily well determined. Consequently, we have used the stars in common between the set of five masks to determine relative mean velocities for each mask, and then assumed that after correction for the mean mask-to-mask offsets, the mean velocity of the likely members on each mask corresponds to the cluster velocity given in the Harris (1996) catalogue. In detail, the velocities were placed on a uniform system by adjusting those for mask 1 by -15 km s^{-1} and those for mask 5 by $+7\text{ km s}^{-1}$ while leaving those for masks 2, 3 and 4 unaltered. A final overall correction of $+37\text{ km s}^{-1}$ (equivalent to a shift of 1.5 pixels) was then applied to place all the velocities on a system that reproduces the Harris (1996) catalogue velocity for the cluster.

Two independent checks of this process are possible. First, there are six stars observed with GMOS-S that were also observed in Saviane et al. (2012). For these stars the mean velocity difference between the GMOS-S and Saviane et al. (2012) observations is -13 km s^{-1} with a standard deviation of 10.2 km s^{-1} . Given that Saviane et al. (2012) suggest velocity errors of $\sim 5\text{--}6\text{ km s}^{-1}$, the standard deviation indicates that the GMOS-S velocity errors are of similar size. The offset, not surprisingly given the way the GMOS-S velocities have been adjusted, accounts for the difference between the mean velocity found for NGC 5824 in Saviane et al. (2012) and that in the Harris (1996) catalogue. The second check is provided by a comparison of the velocities for the 25 stars that have a radial velocity determination from both the GMOS-S observations and from the current FORS2 observations. These stars have a reassuringly low mean velocity difference (GMOS-S – FORS2) of 4.2 km s^{-1} and a standard deviation of 13.8 km s^{-1} . Ascribing the errors equally indicates individual velocity errors are of order $9\text{--}10\text{ km s}^{-1}$, which is sufficient to allow use as a membership criterion. This is discussed further in section 3.2.

2.4 Line Strength Analysis

The strengths of the $\lambda 8542\text{\AA}$ and $\lambda 8662\text{\AA}$ lines of the Ca II triplet were measured on both the GMOS-S and the FORS2 spectra using identical techniques to those described in Saviane et al. (2012). In Fig. 4 we show a comparison of the summed line strengths (ΣW) for the NGC 5824 stars observed in Saviane et al. (2012) with those derived from our new FORS2 observation that employed the identical FORS2 slit configuration. The agreement between the two data sets is excellent with the mean difference between the values of ΣW being 0.06\AA , in the sense Saviane et al. (2012) minus the new determinations. The standard deviation of the differences, 0.17\AA , is consistent with that expected from the measurement errors. We can therefore be confident that line strength measurements made from the new FORS2 spectra are consistent with those in Saviane et al. (2012). In particular, we can directly apply the abundance calibration developed in Saviane et al. (2012) to the new FORS2 data.

The situation for the GMOS-S line strength measurements is, unfortunately, not so clear cut. In Fig. 5 we show the difference between the ΣW values for the spectra centered at $\lambda 8600\text{\AA}$ and for the spectra centered at $\lambda 8550\text{\AA}$, as a function of the average signal-to-noise (S/N) of the spectra. We note that since the $\lambda 8550\text{\AA}$ observations for Mask 4 were impacted by cloud, the comparison is possible only for the brighter stars observed with this mask. Similarly, the comparison is not possible for the small number of stars where either the $\lambda 8542$ or the $\lambda 8662$ line fell in an inter-chip gap on one of the individual spectra. The S/N of each spectra was calculated from the mean and the standard deviation of the counts in the wavelength region $\lambda \lambda 8557\text{--}8647\text{\AA}$ (i.e., between the two stronger triplet lines). This wavelength region is relatively free of stellar absorption lines and the approach takes into account the effect of residual fringing, which reduces the S/N below that which would be inferred from the continuum count level alone.

Figure 5 shows that for most stars there is reasonable agreement between the two measurements of ΣW , partic-

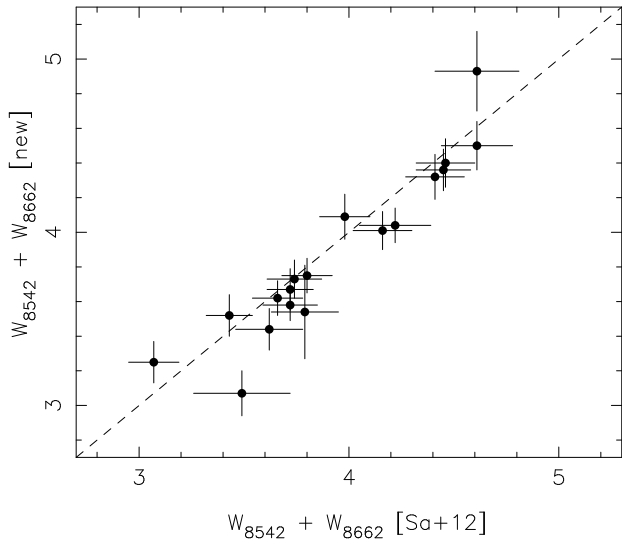


Figure 4. The sum of the equivalent widths of the $\lambda 8542\text{\AA}$ and $\lambda 8662\text{\AA}$ lines of the Ca II triplet (ΣW) as measured from the new FORS2 observations are plotted against the original values from Saviane et al. (2012) for the 18 NGC 5824 members, one non-member stars in common. The dashed line indicates 1:1 correspondence and the error bars are those returned by the line strength measurement code.

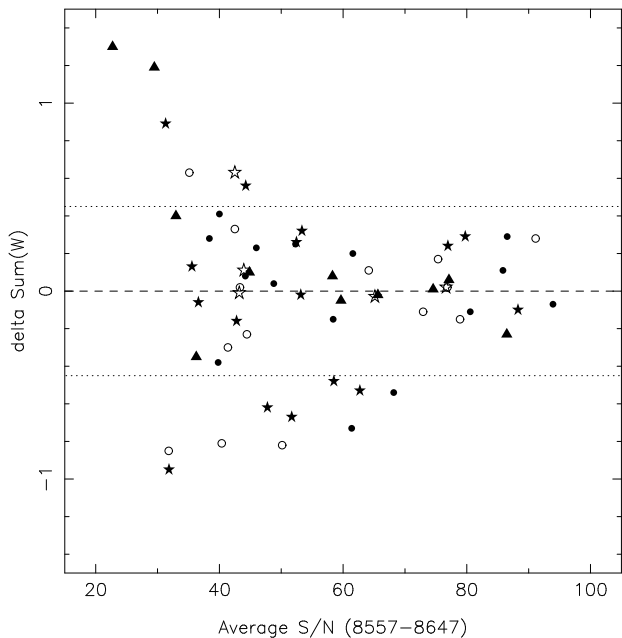


Figure 5. The differences in summed equivalent widths of the $\lambda 8542\text{\AA}$ and $\lambda 8662\text{\AA}$ Ca II triplet lines between measurements made on GMOS-S spectra centered at $\lambda 8600\text{\AA}$, and those made on spectra centered at $\lambda 8550\text{\AA}$, are plotted against the average signal-to-noise (S/N) for each pair of spectra. The S/N values are computed over the wavelength interval $\lambda 8557\text{--}8647\text{\AA}$. Stars from Mask 1 are shown as filled circles, Mask 2 as filled stars, Mask 3 as open circles, and Mask 5 as filled triangles, respectively. The dashed line indicates equality and the dotted lines are $\pm 0.45\text{\AA}$; stars lying outside these lines have not been included in the subsequent analysis.

ularly for the higher S/N spectra. However, there are also stars where the difference is substantial despite apparently good S/N values. In these cases the residual fringing has most likely affected either the line profile or the continuum level resulting in an uncertain line strength measurement. Consequently, we have excluded from the subsequent analysis all stars observed with GMOS-S for which the absolute value of the difference between the two ΣW values exceeds 0.45\AA : within this limit the uncertainty in the average of the two determinations is nominally less than 0.23\AA , which is the largest ΣW error given in Saviane et al. (2012) for their NGC 5824 members. This cut reduces the GMOS-S sample to 45 spectra of 37 stars but given the science aim of the program, the increased confidence in the reliability of the line strength measures outweighs the reduction in sample size. For the 45 spectra pairs with $\Delta(\Sigma W) \leq 0.45\text{\AA}$, the mean difference is 0.05\AA with a standard deviation of 0.20\AA . The lack of any significant difference between the ΣW measures from the two sets of spectra indicates that they can be meaningfully averaged, and all subsequent use of the GMOS-S ΣW values refers to the averaged value.

We can now compare the GMOS-S ΣW values with those from the FORS2 data. There are 5 stars in the remaining GMOS-S sample that are also in Saviane et al. (2012). After applying a line strength correction factor of 1.046 to the GMOS-S values (see Saviane et al. 2012), the five stars have a mean difference in ΣW , in the sense Saviane et al. (2012) minus the GMOS-S determinations, of -0.01\AA . The standard deviation of the differences, 0.10\AA , is again consistent with that expected from the measurement errors. This suggests that the corrected GMOS-S values are on the system defined in Saviane et al. (2012), but a more meaningful comparison is provided by the 19 stars that are in common between the culled GMOS-S sample and the new set of FORS2 observations. This comparison is shown in Fig. 6 where it is clear that a 1:1 line is consistent with the measurements. The mean difference in ΣW , in the sense of the current FORS2 measures minus the corrected GMOS-S measures, is -0.07\AA with a standard deviation of 0.17\AA . A formal least-squares fit to these data has a slope of $1.03 \pm 0.09 \text{ \AA per \AA}$, an intercept of $-0.03 \pm 0.32 \text{ \AA}$, and an *rms* of 0.17 \AA . We conclude therefore that the corrected GMOS-S ΣW measurements are on the same system as the current FORS2 values and both are consistent with that established in Saviane et al. (2012).

3 CLUSTER MEMBERSHIP

In order to fully evaluate the existence of an internal [Fe/H] range in NGC 5824, it is necessary to have a sample of stars for which the membership status is as unambiguous as possible. For many clusters such a task is relatively straightforward because the heliocentric radial velocity of the cluster is sufficiently different from the velocities of non-member field stars that member/non-member classification is readily achieved. This is not the case for NGC 5824 as the relatively low velocity ($-27.5 \pm 1.5 \text{ km s}^{-1}$, Harris (1996)) does not offer much discrimination against field stars. Consequently, we have made use of a series of membership criteria in determining our final sample of NGC 5824 red giant members. We now discuss these criteria in turn.

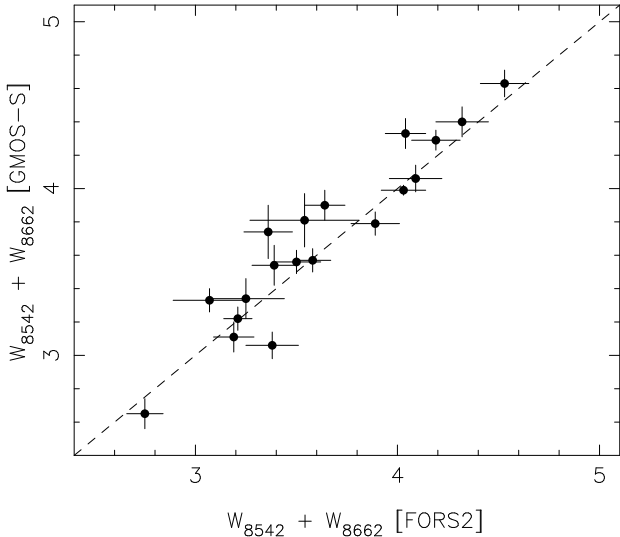


Figure 6. The corrected line strengths from the GMOS-S spectra are plotted against the line strengths from the current FORS2 spectra for the 19 stars in common between the two data sets. The dashed line shows 1:1 correspondence and the error bars are those returned by the line strength measurement code.

3.1 Use of the 8807 Mg I Line

In a recent paper Battaglia & Starkenburg (2012) showed that the strength of the $\lambda 8806.8\text{\AA}$ Mg I line, which is gravity sensitive and stronger in dwarfs than in giants, could be used in conjunction with the equivalent widths of the Ca II triplet lines to effectively discriminate metal-poor red giants from foreground dwarfs. The FORS2 spectra obtained here generally have sufficient S/N that the $\lambda 8807\text{\AA}$ Mg I line could be straightforwardly measured on the spectra with the same gaussian-fitting code used for the Ca II triplet line strength measurements. Unfortunately this was not the case for the GMOS-S spectra where the residual fringing meant that the continuum could not be well enough defined for a sensible measurement of the line strength.

In Fig. 7 we show the strength of the Mg I $\lambda 8807\text{\AA}$ line against ΣW for 163 of the stars observed with FORS2 (Mg I line strengths could not be measured for 9 FORS2 stars). As found by Battaglia & Starkenburg (2012) there are clearly a significant number of stars with relatively large Mg I equivalent widths, which are presumably foreground dwarfs, together with a population showing relatively weak Mg I and Ca II line strengths. These latter stars are presumably predominantly metal-poor giant members of NGC 5824. After considering the location of the brightest probable cluster red giants in this diagram, candidate members of NGC 5824 were selected as having Mg I line strengths weaker than 0.35\AA and ΣW values less than 4.65\AA . The sole exception is star 52005547 for which the Mg I line strength measurement is quite uncertain. This star was retained as a possible member, as were the 9 FORS2 stars without a Mg I measurement and the 18 stars in the GMOS-S sample not also in the FORS2 sample, leaving a reduced sample of 148 stars.

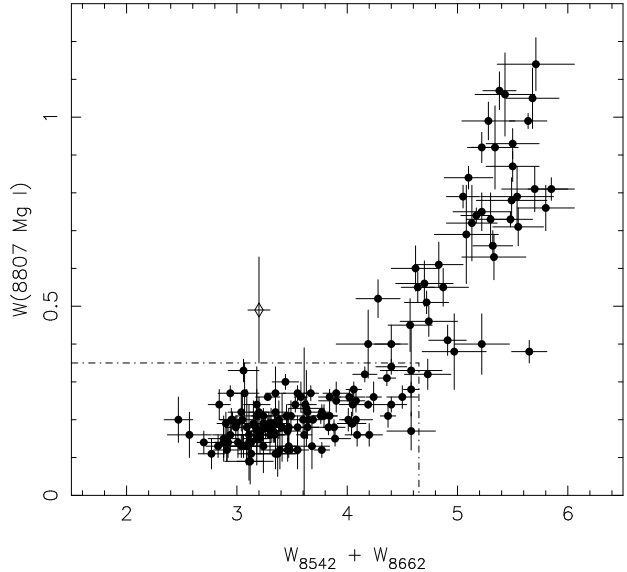


Figure 7. The equivalent width of the $\lambda 8807\text{\AA}$ Mg I line, $W(8807\text{ Mg I})$, is plotted against the sum of the equivalent widths of the $\lambda 8542\text{\AA}$ and $\lambda 8662\text{\AA}$ Ca II lines, $W_{8542}+W_{8662}$, for 163 stars observed with FORS2. The stars inside the region outlined by the dot-dash lines are considered possible cluster members while the stars outside the region are classified as non-members. The star (52005547) with a relatively weak $W_{8542}+W_{8662}$ and intermediate but uncertain $W(8807\text{ Mg I})$ value, shown by the open diamond symbol, is also included in the possible member sample.

3.2 Radial Velocities

Inspection of the radial velocities of the 148 stars that passed the Mg I selection criteria reveals one obvious outlier – star 62000110 with a velocity of $+288\text{ km s}^{-1}$. The radial velocities of the remaining 147 stars are plotted against ΣW in Fig. 8. Consideration of this figure suggests two further non-members: stars 12002438 and 41001292 which are plotted as open symbols in Fig. 8. The velocities of these two stars are notably lower than those of the rest of the sample. Excluding these two stars the 145 remaining candidate members (shown as filled symbols) have mean velocity of -28.9 km s^{-1} and a standard deviation σ_v of 11.7 km s^{-1} . Both 12002438 and 41001292 then lie further than $3\sigma_v$ from the mean. The value of σ_v is consistent with the combination of the individual velocity errors ($9\text{--}10\text{ km s}^{-1}$, see §2.3.2) and a radial decrease in the intrinsic velocity of dispersion of NGC 5824 stars from the central value of $11 \pm 2\text{ km s}^{-1}$ (Dubath et al. 1997). The mean velocity for the sample of $-28.9 \pm 1.0\text{ km s}^{-1}$ is fully consistent with the value of $-27.5 \pm 1.5\text{ km s}^{-1}$ listed in the Harris (1996) catalogue.

3.3 Color-Magnitude Diagram

In Fig. 9 we show the CMD for the candidate NGC 5824 members that have passed the (Mg I, ΣW) line strength (where a Mg I line strength has been measured) and radial velocity selection criteria. We note first that, as is immediately apparent from the figure, there exist a sizeable number of stars that lie away from the cluster RGB in the CMD. Many of these were included in the FORS2 observations in order to ensure a broad colour selection to prevent any

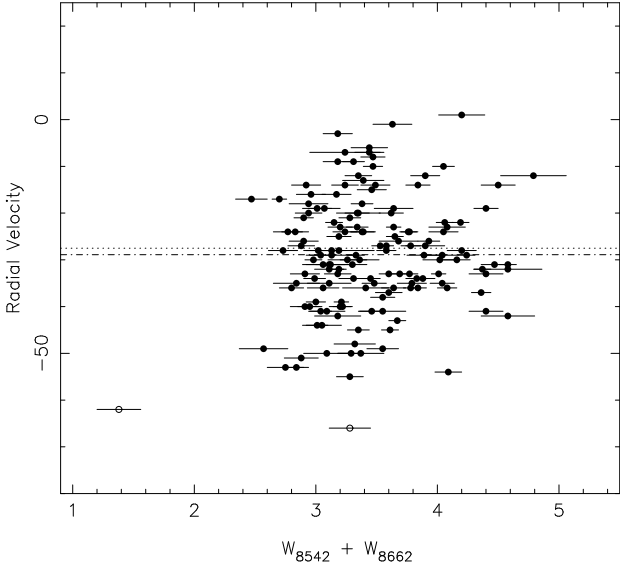


Figure 8. Heliocentric radial velocity is plotted against the sum of the equivalent widths of the $\lambda 8542\text{\AA}$ and $\lambda 8662\text{\AA}$ Ca II lines, $W_{8542} + W_{8662}$, for the all the stars observed except those excluded from cluster membership via Fig. 7. Probable cluster members are shown as filled symbols while the open symbols show stars considered probable non-members on the basis of their velocity. The dot-dash line shows the mean velocity of the 145 probable members while the dotted line shows the Harris (1996) catalogue velocity.

bias in the $[\text{Fe}/\text{H}]$ determinations. A number of these stars are clearly asymptotic giant branch (AGB) members of the cluster. Because of their lower mass, AGB stars have lower gravities than RGB stars and at the same colour, or effective temperature, AGB stars are also brighter than RGB stars. This offset can be significant at luminosities fainter than the vicinity of the RGB tip. Consequently, it is clear that AGB stars will occupy a different location in the customary line strength analysis plot (e.g., Saviane et al. 2012), which uses $V - V_{HB}$ as the abscissa, even if the actual abundance of the AGB stars is the same as that for the RGB stars. We have therefore visually identified 33 AGB star candidate members in the CMD of Fig. 9, and these stars are shown as open symbols. Shown also on the figure is a fit of a fourth order polynomial to the RGB stars that defines the locus of the mean RGB in the CMD. The line-strength analysis is then restricted to the 112 RGB candidate members.

3.4 Line Strength Diagram

The sum of the equivalent widths of the $\lambda 8542\text{\AA}$ and the $\lambda 8662\text{\AA}$ Ca II triplet lines, ΣW , is plotted against magnitude difference from the horizontal branch, $V - V_{HB}$, for the 112 candidate RGB members of NGC 5824 in Fig. 10. Shown also on the plot as dashed lines are the (line strength, magnitude) relations for abundances $[\text{Fe}/\text{H}] = -2.3$, -2.0 and -1.7 dex as implied by the abundance calibration derived in Saviane et al. (2012). Four stars stand out as having line strengths notably stronger than the rest of the sample. As inferred from Fig. 10 these stars have abundances of $[\text{Fe}/\text{H}] \approx -1.7$ dex or larger and should therefore lie to the red of the mean RGB in Fig. 9. However, this is not the case —

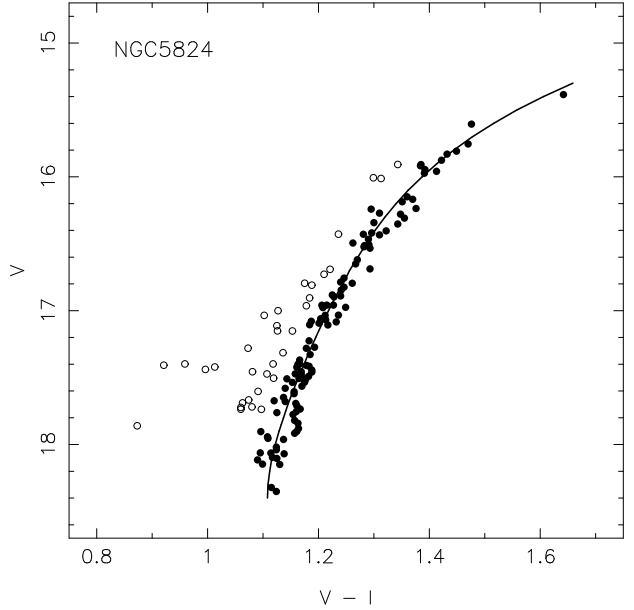


Figure 9. Color-magnitude diagram for the 145 NGC 5824 probable cluster members that satisfy the (Mg I, Ca II) line strength and radial velocity criteria. Filled circles are used for candidate members on the RGB and open circles for candidate AGB members. The solid line is a fourth order polynomial fit to the RGB stars.

all four lie within the dispersion about the mean RGB. Consequently, we shall assume that these four stars (41001144, 42006240, 42011950 and 61002588) are not cluster members and not consider them further. We note, however, that the star 42006240 is star 2_32429 in the Saviane et al. (2012) study and was considered a cluster member in that work. The final sample is then 108 RGB candidate members.

For completeness we note that the equivalent plot to Fig. 10 for the AGB stars identified in Fig. 9 shows that all the stars, with the sole exception of star 61000920, have line strengths that are consistent with cluster membership. Star 61000920 has a much larger $W_{8542} + W_{8662}$ value than the other AGB stars with similar $V - V_{HB}$ and is thus unlikely to be a cluster member. We also note that, as expected, the mean line through the AGB data points is $\sim 0.4\text{\AA}$ weaker at fixed $V - V_{HB}$ compared to the equivalent relation for the RGB stars.

In Table 1 we list the identification number, position, photometry, line strength measurements and additional information for the entire sample of 190 stars observed at both the VLT and Gemini-S.

4 ANALYSIS

In a process identical to that followed in Saviane et al. (2012), an unweighted fit of a line with slope $-0.627\text{\AA}/\text{mag}$ to the final sample of NGC 5824 RGB stars in Fig. 10 yields a $\langle W' \rangle$ value of 2.62\AA , with a standard deviation of the mean of 0.02\AA . Using the abundance calibration given in Saviane et al. (2012), this yields a mean abundance for NGC 5824 of $[\text{Fe}/\text{H}] = -2.01 \pm 0.13$, where the uncertainty is dominated by that of the calibration relation. This abundance is in fact identical to that found in

Table 1. NGC 5824 Stars Observed^e

ID	RA (2000)	Dec (2000)	V	$V - I$	Rad Vel (km s ⁻¹)	$\Sigma(W)^a$ (Å)	error (Å)	W_{8807} (Å)	error (Å)	N_F^b	N_G^c	Class ^d
11000467	226.10370	-33.06391	17.433	0.952	+95	4.28	0.20	0.52	0.05	1	0	NM
11000781	226.13540	-33.05518	16.471	1.152	-46	5.28	0.24	0.99	0.05	1	0	NM
11001198	226.06163	-33.04313	16.352	1.343	-14	3.84	0.10	0.26	0.02	1	0	MR
11001586	226.11004	-33.02972	17.897	0.953	-50	4.64	0.15	0.55	0.04	3	0	NM

Notes. ^a $W_{8542} + W_{8662}$. ^bNumber of observations with FORS2 at the VLT. ^cNumber of observations with GMOS-S at Gemini South. ^dMR indicates star is member of the final RGB sample, MA for stars in the final AGB member sample, and NM for probable non-member of the cluster. ^eThis table is available in its entirety in a machine-readable form in the online journal. A portion is shown here for guidance regarding its form and content.

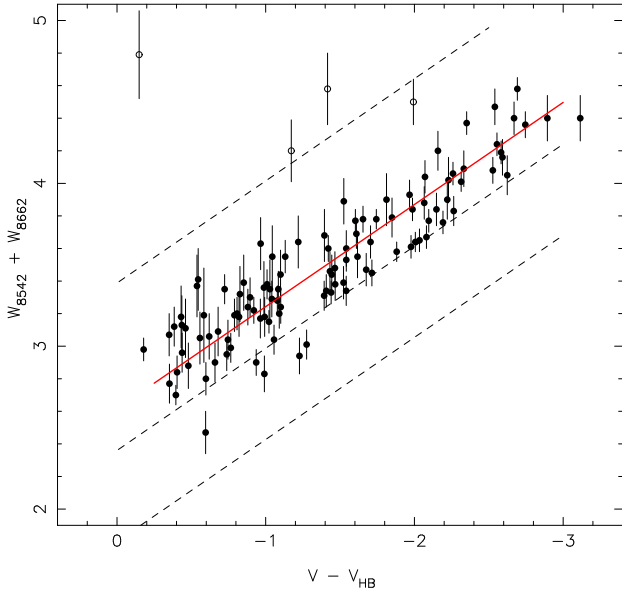


Figure 10. Sum of the equivalent widths of the $\lambda 8542\text{\AA}$ and $\lambda 8662\text{\AA}$ lines of the Ca II triplet is plotted against $V - V_{HB}$ for the 112 candidate RGB members of NGC 5824. Four stars that have line strengths substantially stronger than the other stars are plotted as open-symbols. These stars are probably not cluster members. The dashed lines show the relation between line strength and $V - V_{HB}$ for abundances of $[\text{Fe}/\text{H}] = -2.3, -2.1$ and -1.7 dex using the calibration of Saviane et al. (2012). The solid red line is the fit to the filled symbol points and corresponds to a mean abundance for NGC 5824 of $[\text{Fe}/\text{H}] = -2.01$ dex.

Saviane et al. (2012). Again following the same procedures as Saviane et al. (2012), the *rms* dispersion about the fitted line is 0.19 \AA while the mean of the errors returned by the measurement code, is significantly smaller, at 0.11 \AA . This implies an intrinsic dispersion in the line strengths of 0.15 \AA , or $\sigma_{int}([\text{Fe}/\text{H}]) = 0.06$ dex. This value is lower than that, 0.12 dex, found in Saviane et al. (2012) from a sample of 17 stars, as against the 108 employed here. As noted in Saviane et al. (2012), the largest contribution to their *rms* dispersion came from two stars: 2.32429 (42006240), which we now consider a non-member, and 1.8575 (42013479) whose line strength is measured here as $\sim 0.4 \text{ \AA}$ less than the value given in Saviane et al. (2012). Removing these two stars from the Saviane et al. (2012) dataset then results in an intrinsic line strength dispersion of 0.16 \AA , which is then completely consistent with the new value found here. We conclude that Saviane et al. (2012) were correct in reporting that NGC 5824 possesses an intrinsic $[\text{Fe}/\text{H}]$ range, al-

though the size of the intrinsic dispersion measured here is considerably smaller.

The above analysis assumes that the line strength errors returned by the measurement code are a reasonable estimate of the true errors. Saviane et al. (2012) adopted this assumption but with these new data we can make use of the stars with repeat spectra to gain an independent assessment of the line strength measurement errors as a function of signal-to-noise. For the FORS2 spectra, there are 40 stars with at least two observations and we estimate the error in a single FORS2 measurement of ΣW as follows. The error estimate for a single observation is calculated using the formalism of Keeping (1995) in which the error is given by the expression $k \times |\Delta W|$, where $|\Delta W|$ is the range of the equivalent width measures for a given star and k is a constant that depends on the number of observations, e.g., for two observations $k = 0.886$. In Fig. 11 this single observation error estimate is plotted against the average signal-to-noise in the wavelength region $\lambda\lambda 8557\text{--}8647\text{\AA}$ for the 40 stars with at least two FORS2 observations. As noted above, this wavelength region, which lies between the two stronger Ca II triplet lines, is relatively free of stellar absorption lines and the S/N provides a good measure of the quality of the spectrum. Shown also on the figure are two exponential curves which outline the adopted upper and lower envelopes to the data points. These have been derived via a least squares fit to the $[\text{S}/\text{N}, \ln(\text{error estimate})]$ data to determine the exponent, with the amplitude then increased and decreased to encompass the majority of the points. For stars with FORS2 spectra, we then assume that at a given signal-to-noise, the error for an individual star is uniformly distributed between the upper and lower limits in the figure.

Similarly, for the Gemini spectra we use the equivalent plot (cf. Fig. 5) to assess the likely errors in the measurements of the summed equivalent widths, and again assume that the errors are uniformly distributed between upper and lower boundaries that are a function of the signal-to-noise. For multiply observed stars within each sample, the estimated error is reduced by the square root of the number of observations, while for stars observed with both GMOS-S and FORS2, the uncertainty is that of (unweighted) mean. Within the FORS2 sample there are 9 stars⁴ with computed $\text{S}/\text{N} \leq 50$, beyond the limits of the exponential envelope curves in Fig. 11. We have not considered these stars further leaving a final sample of 99 NGC 5824 red giants. We

⁴ The stars are 31003802, 32004263, 42007205, 42007589, 51001013, 52005984, 52010221, 61000102 and 61000435.

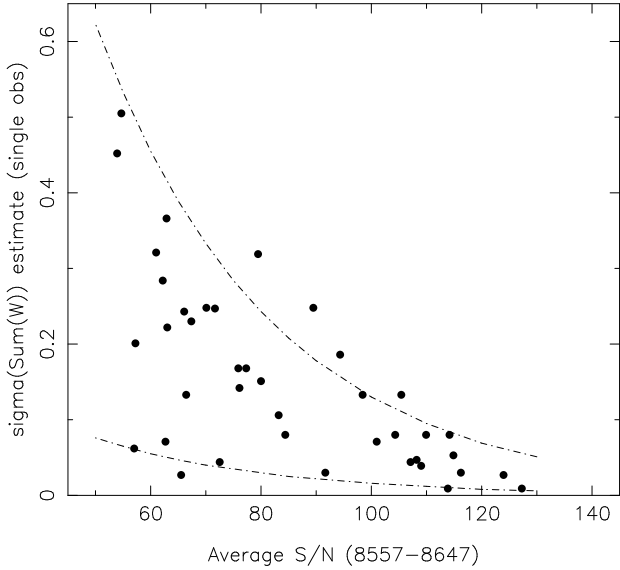


Figure 11. Estimates of the error in the summed equivalent width of the $\lambda 8542\text{\AA}$ and $\lambda 8662\text{\AA}$ Ca II triplet lines for a single FORS2 observation as a function of the signal-to-noise ratio in the wavelength region $\lambda\lambda 8557\text{--}8647\text{\AA}$. The filled circles are estimates from the stars which have at least two FORS2 observations. The dot-dash curves are exponentials that define the adopted upper and lower envelopes to the data points.

can now simulate the effect of the measurement errors on the summed equivalent width determinations, and hence on the abundance distribution.

In Fig. 12 we show the outcome of 1000 trials in which the observed summed equivalent widths are translated directly to metallicity, with errors assigned as described above. The red line is the mean generalized histogram from these trials while the grey curves represent the $\pm 3\sigma$ deviates about the mean. As a comparison, we assume as a null hypothesis that the cluster has a single metallicity equal to the mean determined above and that the error for each star is the absolute value of the difference between the observed summed equivalent width and the value expected for the mean abundance at the $(V - V_{HB})$ of the star. The generalised histogram under this assumption is shown as the blue line. In both cases the minimum error in $[\text{Fe}/\text{H}]$ has been taken as 0.015 dex in order to minimise the influence on the overall histograms of δ -function-like spikes, which can occur if the error in $[\text{Fe}/\text{H}]$ becomes unrealistically small. The exact value of this limit, within the range 0.010 – 0.020 dex, does not affect the interpretation of the histograms.

It is clear from Fig. 12, that even allowing for the $\pm 3\sigma$ deviates, the two assumptions provide curves that are significantly different, confirming that NGC 5824 does indeed possess an intrinsic dispersion in $[\text{Fe}/\text{H}]$. We can characterise the distribution shown by the red curve in Fig. 12 in a number of ways; for example, the FWHM of the distribution is 0.16 dex. Alternatively, using the abundance determinations themselves, the inter-quartile range (IQR) of the sample is 0.10 dex and the total range in $[\text{Fe}/\text{H}]$ is ~ 0.30 dex. We have also investigated whether any correlation is present between the deviations in line strength at fixed $V - V_{HB}$ from the mean relation in Fig. 10 and deviations in $(V - I)$ colour at fixed V from the mean red giant branch in Fig. 9. No

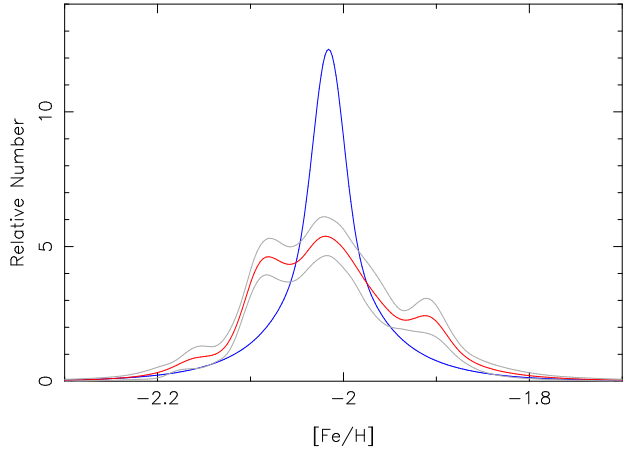


Figure 12. Generalized histograms representing abundance distributions derived from the observed summed equivalent width values. The red curve is the mean generalized histogram assuming that the measured summed equivalent widths translate directly to abundance $[\text{Fe}/\text{H}]$, while the grey curves show the $\pm 3\sigma$ deviates about the mean from the sampling of the measurement errors. The blue curve is the mean generalized histogram under the assumption that there is no intrinsic abundance dispersion among the NGC 5824 red giants.

convincing correlation is present. This lack of a correlation, however, is not surprising given the small size of the abundance dispersion and the comparative lack of sensitivity of RGB colour to abundance at low abundances. For example, using the Dartmouth isochrones (Dotter et al. 2008), the difference in $(V - I)$ at $V = 16.0$ ($V - V_{HB} = -2.5$) between an RGB with $[\text{Fe}/\text{H}] = -2.1$ and one with $[\text{Fe}/\text{H}] = -1.9$ is only 0.033 mag, while at $V = 17.5$ ($V - V_{HB} = -1.0$), the difference is even smaller, 0.013 mag. Intrinsic colour differences of this order are simply too small to convincingly detect given the errors in the photometry.

Fig. 12 also shows that NGC 5824 abundance distribution is apparently not unimodal – the red solid line in the figure shows three distinct peaks that correspond to abundances of $[\text{Fe}/\text{H}] \approx -2.09, -2.01$ and -1.91 dex, with approximately equal numbers in the first two groups and a smaller population in the third more metal-rich group. We have endeavoured to model this observed distribution to investigate its implications. The modeling has been carried out by randomly selecting 99 abundances (corresponding to the number of stars in the final observed RGB sample) from an assumed input abundance distribution, and assigning errors to these abundances in the same way as for the observed stars allowing computation of a generalised histogram. The selection process is then repeated 1000 times and the mean generalised histogram for the model calculated. A model is then accepted as a satisfactory fit to the observations if the model mean generalised histogram is contained entirely within the $\pm 3\sigma$ limits of the observational data histogram shown in Fig. 12.

Examples of this process are shown in the panels of Fig. 13. In the upper panel the adopted input abundance distribution has three components: the first has a single abundance of $[\text{Fe}/\text{H}] = -2.09$ and comprises 25% of the total, the second has abundances uniformly distributed between $[\text{Fe}/\text{H}] = -2.06$ and -1.97 and comprises 60% of the total,

and the third has a fixed abundance of $[\text{Fe}/\text{H}] = -1.91$ and 15% of the total. Effectively by construction this model does an acceptable job of reproducing the three apparent peaks in the observed abundance distribution. In this context it is worth noting that with this type of three component model it was not possible to achieve an acceptable fit in the case where the three components each had discrete abundances. We must, however, be careful not to over-interpret the outcomes of this heuristic model fitting. For example, we show in the lower panel of Fig. 13 a model which also provides an acceptable fit to the observed data and which does not contain any discrete components. For this model 80% of the population is assumed to have metallicities distributed uniformly between $[\text{Fe}/\text{H}] = -2.11$ and -1.97 dex, while the remaining 20% have metallicities drawn from a distribution that decreases linearly from matching the uniform population relative number at $[\text{Fe}/\text{H}] = -1.97$ to zero at $[\text{Fe}/\text{H}] = -1.87$ dex.

There are nevertheless robust conclusions that can be drawn from the modeling process aside from the obvious one that an intrinsic abundance spread is required. The first is that on the metal-poor side the abundance distribution must rise rapidly with increasing abundance. It is not possible to determine whether a particular abundance cut-off near $[\text{Fe}/\text{H}] \approx -2.1$ is required, below which no stars are found, or whether there is simply a very rapid increase in numbers above this abundance, but a feature of this nature is required. A sharp rise in the metallicity distribution function on the metal-poor side is reminiscent of the abundance distributions in clusters such as ω Cen and M22 (see Da Costa et al. (2009) and Fig. 1 in Da Costa & Marino (2011)). In this respect these star cluster abundance distributions contrast strongly with those for dwarf galaxies where the abundance distributions show much less steep increases with increasing metallicity on the metal-poor side of the distribution (see for example, Fig. 17 in Norris et al. 2010). In contrast to the metal-poor side, the metal-rich side of the NGC 5824 abundance distribution declines more slowly but the extent of the metal-richer population is less than for M22 and much less than for ω Cen.

The second conclusion that can be drawn from the modeling process is that distributions with strong single peaks, such as a Gaussian, provide a poor representation of the observations. Instead, the observations suggest input distributions that are more “flat-topped”, either as discrete components of approximately similar strength or more uniform distributions such as the model used to generate the lower panel of Fig. 13. Unfortunately, given the sample size observed here, it is unlikely that further progress can be made in characterising the NGC 5824 abundance distribution until a comparable number of precise $[\text{Fe}/\text{H}]$ determinations are made using high dispersion spectroscopy.

One additional point, however, needs to be discussed. NGC 2419 is a luminous outer halo globular cluster whose overall abundance, $[\text{Fe}/\text{H}] = -2.09$ (e.g., Mucciarelli et al. 2012), is similar to that for NGC 5824. Mucciarelli et al. (2012) have shown that while NGC 2419 does show large anti-correlated variations in Mg and K abundances, it apparently does not possess an intrinsic range in $[\text{Fe}/\text{H}]$ or $[\text{Ca}/\text{H}]$ (Mucciarelli et al. 2012). This is despite initial suggestions to the contrary (e.g., Cohen et al. 2010), which were based on analysis of Ca triplet line strengths. Mucciarelli et al.

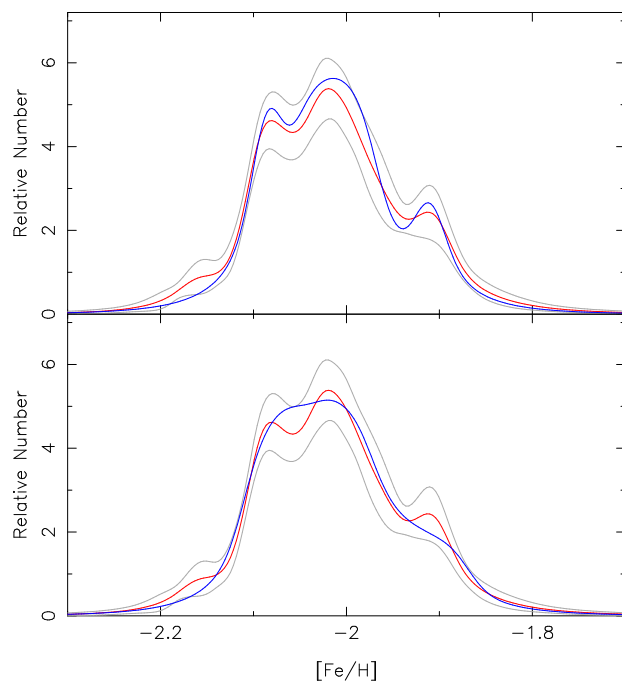


Figure 13. As for Fig. 12 the red curve is the mean generalized histogram for the observations, generated by assuming the measured summed equivalent widths translate directly to abundance $[\text{Fe}/\text{H}]$. The grey curves show the $\pm 3\sigma$ deviates about the mean from the sampling of the measurement errors. In the *upper panel* the blue curve is the mean generalized histogram resulting from a model which assumes that there are three separate populations in the cluster: one with $[\text{Fe}/\text{H}] = -2.09$ comprising 25% of the total, a second with abundances uniformly distributed between $[\text{Fe}/\text{H}] = -2.06$ and -1.97 and 60% of the total, and a third with $[\text{Fe}/\text{H}] = -1.91$ and 15% of the total. The *lower panel* shows with the blue curve the mean generalised histogram for an alternate model. In this model the abundances for 80% of the population are distributed uniformly between $[\text{Fe}/\text{H}] = -2.11$ and -1.97 dex, while the remaining 20% have metallicities drawn from a distribution that decreases linearly from matching the uniform population relative number at $[\text{Fe}/\text{H}] = -1.97$ to zero at $[\text{Fe}/\text{H}] = -1.87$ dex.

(2012) instead ascribe the observed variations in the Ca triplet line strengths to opacity differences that result from variations in the abundance of the electron-donor element Mg: the Mg deficient stars consequently show stronger $\lambda 8542\text{\AA}$ and $\lambda 8662\text{\AA}$ Ca lines and vice versa without any true variation in $[\text{Ca}/\text{H}]$ or $[\text{Fe}/\text{H}]$. Therefore, given these results for NGC 2419, it is necessary for us to check that our inferred Ca triplet line strength spread is due to a real spread in Ca (and Fe) abundances rather than to an opacity effect.

We have carried out this check by investigating the strength of the $\lambda 8688.6\text{\AA}$ Fe I line and of the $\lambda 8806.7\text{\AA}$ Mg I line as a function of ΣW . We considered only the brighter RGB stars, those with $(V - V_{HB}) \leq -2.0$, and with FORS2 spectra, in order to maximise the signal-to-noise of the measurements. The Fe I line was measured via gaussian fitting using the same continuum regions as for the $\lambda 8662\text{\AA}$ Ca triplet line. If the NGC 2419 effect was also present in NGC 5824 then we would expect the red giants with stronger Ca triplet lines to have weaker Mg I lines at fixed $(V - V_{HB})$, and vice versa, and for there to be no intrinsic

sic scatter in the iron line strengths about any mean trend with $(V - V_{HB})$. We find from our measurements that firstly, there is only marginal support for any anti-correlation between ΣW and the strength of the Mg I $\lambda 8807\text{\AA}$ line. After removing a (small) trend with $V - V_{HB}$, we find that the stars with weaker Ca triplet lines have stronger Mg I lines at only the $\sim 1\sigma$ level (5 ‘weak’ stars versus 3 ‘strong’ stars from a full sample of 22 objects). Secondly, and more significantly, we find, again after removing a small trend with $V - V_{HB}$, that the stars with stronger Ca II lines do indeed have stronger $\lambda 8688.6\text{\AA}$ Fe I lines, at the 2σ level, compared to the stars with weaker Ca II lines. Consequently, while the outcome is undoubtedly limited by the signal-to-noise of the spectra and the weakness of the Mg I and Fe I lines (typical measured equivalent widths of 0.24\AA and 0.18\AA , respectively), we see no compelling reason to suggest that the observed intrinsic variation in Ca triplet lines among the red giants in NGC 5824 is anything else other than the result of an intrinsic overall abundance dispersion in this cluster.

5 DISCUSSION

With our results NGC 5824 joins the small list of Galactic globular clusters that possess sizeable intrinsic $[\text{Fe}/\text{H}]$ abundance dispersions⁵. As noted in the Introduction this list also includes ω Cen, M54, M22, NGC 1851 and perhaps NGC 3201 (see §1 for references); we again choose to exclude the metal-rich Galactic Bulge cluster Terzan 5 from this list given that the large difference in abundance between the two distinct stellar populations present in the cluster (Origlia et al. 2011) suggests a different mechanism is involved. In Fig. 14 we show an updated version of the relation between intrinsic $[\text{Fe}/\text{H}]$ dispersion, as measured by the standard deviation of the $[\text{Fe}/\text{H}]$ distribution⁶, and absolute magnitude for Galactic globular clusters. This relation was first discussed in Carretta et al. (2010a, see also Carretta et al. (2009)). In the figure upper limits on intrinsic $[\text{Fe}/\text{H}]$ dispersion values are shown by open symbols; these data are taken directly from Carretta et al. (2009). The filled star-symbols are the clusters (excluding Ter 5) with identified significant intrinsic $[\text{Fe}/\text{H}]$ dispersions, which now include NGC 1851, NGC 3201 and NGC 5824, results that were not available to Carretta et al. (2010a). The plotted value for NGC 3201 comes from the $[\text{Fe}/\text{H}]$ values tabulated by Simmerer et al. (2013) while that for NGC 1851 comes from Carretta et al. (2011). The value for NGC 5824 is the one derived here, while for M22 we use the value derived from the $[\text{Fe}/\text{H}]$ abundances listed in Marino et al. (2011); Da Costa et al. (2009) list a somewhat higher value of $\sigma_{obs}[\text{Fe}/\text{H}] = 0.15$ dex. The other change from the depiction of this figure in Carretta et al. (2010a) is for the cluster NGC 2419. Mucciarelli et al. (2012) have established that

⁵ We note that if studies at the exquisite level of precision obtained by Yong et al. (2013) for NGC 6752 red giants were common, it is conceivable that they would reveal many globular clusters possess intrinsic iron abundance dispersions at the $\sigma_{int}([\text{Fe}/\text{H}]) \lesssim 0.02\text{--}0.03$ dex level.

⁶ The IQR of the distributions would be a better measure to employ here as it makes no assumption about the form of the distribution, but this statistic is not available for all the clusters.

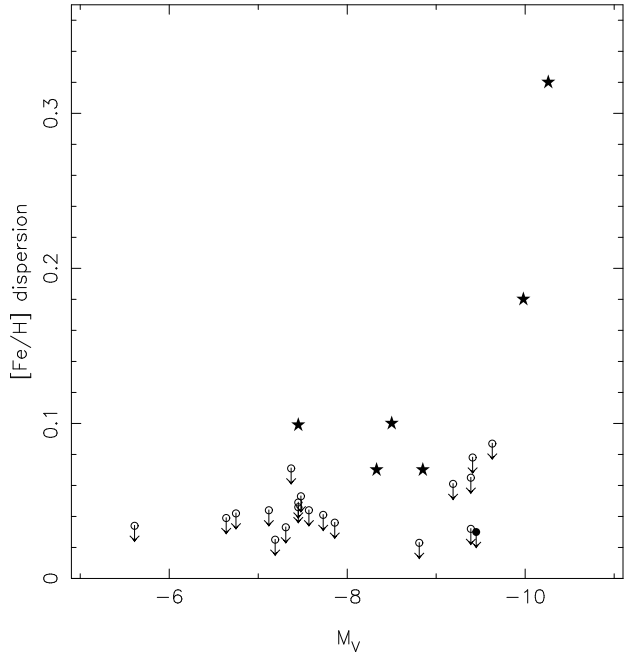


Figure 14. Standard deviation in $[\text{Fe}/\text{H}]$ abundances is plotted against absolute visual magnitude for a number of Galactic globular clusters. The open symbols are upper limits on any intrinsic abundance dispersions and are taken from Carretta et al. (2009). The filled circle is NGC 2419 using the $[\text{Fe}/\text{H}]$ abundance dispersion limit from Mucciarelli et al. (2012). The star-symbols are clusters with measured intrinsic $[\text{Fe}/\text{H}]$ abundance dispersions exceeding 0.05 dex. In order of decreasing absolute magnitude the clusters are ω Cen and M54, from Carretta et al. (2009), NGC 5824 from this work, M22 (Marino et al. 2011), NGC 1851 (Carretta et al. 2011) and NGC 3201 (Simmerer et al. 2013).

the intrinsic $[\text{Fe}/\text{H}]$ abundance range in NGC 2419 is actually small, in contrast to earlier estimates (see the discussion in Mucciarelli et al. 2012).

Although the number of clusters studied is not large, and selection effects are undoubtedly important⁷, there does not seem to be any definite correlation between the size of $\sigma_{int}([\text{Fe}/\text{H}])$ and M_V in Fig. 14, particularly if the Simmerer et al. (2013) results for NGC 3201 are valid. Instead, while ω Cen and M54 clearly stand out in terms of luminosity and size of abundance spread, for the other four clusters with intrinsic spreads the size of the intrinsic dispersion does not clearly change with absolute magnitude. This differs from the suggestion in Carretta et al. (2010a) of an apparently statistically significant relation between the size of the intrinsic iron abundance spread and luminosity. What is apparent from Fig. 14 however, is that the likelihood of an intrinsic abundance dispersion is larger for more luminous clusters: 5 of the 12 clusters in Fig. 14 with $M_V < -8$ show

⁷ For example, Carretta et al. (2009) give an upper limit for the $[\text{Fe}/\text{H}]$ abundance dispersion in NGC 3201 as 0.049 dex and Saviane et al. (2012) also find no evidence for a $[\text{Fe}/\text{H}]$ abundance dispersion in the cluster. Both results contrast with the intrinsic dispersion of 0.10 dex found by Simmerer et al. (2013). A possible explanation for the difference is that the first two studies deliberately selected stars near the mean RGB for observation, while the Simmerer et al. (2013) study is less biased in that respect. See also the discussion in Muñoz et al. (2013).

intrinsic dispersions, while only 1 or none (depending on the reality of the NGC 3201 result) of the 14 less luminous clusters show intrinsic dispersions. Abundance dispersion limits or determinations for a larger sample of clusters are needed to fully explore the implications of this figure.

Nevertheless, we can speculate on a possible interpretation. Given the location of M54 as the nuclear star cluster of the Sagittarius dwarf galaxy, and given the frequently assumed status of ω Cen as the nuclear remnant of a disrupted dwarf galaxy, it is tempting to postulate, as did Saviane et al. (2012), that the other clusters, including NGC 5824, with significant intrinsic [Fe/H] dispersions, i.e., exceeding $\sigma_{int}([\text{Fe}/\text{H}]) \approx 0.05$ dex, are also the remnant central star clusters of tidally disrupted dwarf galaxies. Bekki & Yong (2012) investigated this possibility in the context of NGC 1851 (see also Carretta et al. 2010a), and in the same sense NGC 3201, with its highly retrograde orbit (Casetti-Dinescu et al. 2007) has long been suggested as having originated in an extra-galactic system accreted by the Milky Way (e.g., Rodgers & Paltoglou 1984). As regards ω Cen, M22 and NGC 5824, the steep slope of the metal-poor side of the metallicity distribution is consistent with the rapid enrichment that would be expected to occur in the central regions of a dwarf galaxy during its initial formation. Further evidence to support our speculation lies in the discovery of Olszewski et al. (2009, see also Carballo-Bello et al. (2012)) that NGC 1851 is surrounded by a diffuse envelope of stars whose location in the CMD replicate the cluster main sequence. The diameter of the NGC 1851 envelope is ~ 500 pc, much larger than the nominal tidal radius of the cluster (Olszewski et al. 2009; Carballo-Bello et al. 2012). Olszewski et al. (2009) suggest that the envelope may represent stars lost from the cluster via a variety of dynamical processes, but it could equally represent the remnants of a disrupted dwarf galaxy in which NGC 1851 was (or is) embedded (Olszewski et al. 2009). The situation, however, may be more complex as the spectroscopic follow-up of Sollima et al. (2012) apparently finds evidence not only for a population of NGC 1851 stars beyond the cluster tidal radius, but also for what appears to be an additional stellar stream at a different velocity to that of the extended cluster population.

As noted in the Introduction, Newberg et al. (2009) have suggested a connection between NGC 5824 and the Cetus Polar Stream, which has a similar low metallicity to that of the cluster (Newberg et al. 2009). Regardless of the validity of this possible connection, it is intriguing in this context to note that NGC 5824 is apparently also *surrounded by a large diffuse stellar envelope*. The density profile of the cluster as presented in Grillmair et al. (1995) shows no signs of a tidal cutoff – rather there is a power-law projected density profile that extends well past the nominal tidal radius of $\sim 5.7'$ (Harris 1996). The power-law slope is $r^{-2.2 \pm 0.1}$ and cluster stars are detectable to $\log(r') \approx 1.65$ or $r \approx 45'$ (Grillmair et al. 1995). Carballo-Bello et al. (2012) find similar results. At the 32 kpc distance of NGC 5824 (Harris 1996), a radius of $45'$ corresponds to 420 pc or a diameter approaching one kpc in size. This is almost twice the size of the diffuse envelope surrounding NGC 1851 and approaches the scales of low luminosity dwarf galaxies. For example, Bootes I stars are detected to a radius of ~ 500 pc (Martin et al. 2008). The Grillmair et al. (1995) data also

show some indication that the NGC 5824 diffuse envelope is more extended in the N-S direction than it is in the E-W direction. Given the likely mass of the cluster ($\sim 6 \times 10^6 M_{\odot}$ for $M/L_V = 2$) and the large Galactocentric distance, it is unlikely that tidal effects are responsible for the outer diffuse envelope of NGC 5824, though an origin with internal dynamical processes remains possible, as does the interpretation that the envelope represents a remnant population of a disrupted dwarf galaxy. A deep large area study of this cluster and its surrounds is clearly called for, and is being undertaken by our group. A spectroscopic survey to determine the mean metallicity and metallicity spread of the stars in the diffuse envelope would also be worthwhile as it would constrain any differences between the abundance properties of the putative nuclear star cluster (NGC 5824), where nucleosynthesis processes may have proceeded more quickly, and those of the postulated dwarf galaxy ‘field star’ population.

The results of Lee et al. (2007) are also relevant to the discussion (see also §5.3 of Saviane et al. 2012). Lee et al. (2007) investigated the luminosity distribution and kinematic properties of groups of Galactic globular clusters selected by HB type. Based on a total sample of 114 objects, they found that the 28 clusters with extended horizontal branches (EHB clusters) are notably more luminous than the rest of the sample. The EHB morphology, i.e., a horizontal branch morphology extending to very high temperatures, is thought to be associated with the presence of a cluster stellar population that possesses an enhanced helium abundance (e.g., D’Antona et al. 2005). Further, Lee et al. (2007) showed that the EHB clusters as a group have kinematics that are dominated by random motions lacking any correlation with metallicity. Lee et al. (2007) then use these results to argue that the EHB clusters are a distinct population with an accretion-event origin for most, if not all of the clusters. As regards our sample of six clusters with significant intrinsic [Fe/H] dispersions, three (ω Cen, M54 and M22) belong to the group with strongly extended horizontal branch morphologies, while two (NGC 1851 and NGC 5824) are in the “moderately extended HB” group (Lee et al. 2007). Only NGC 3201 is not a member of the EHB group. Consequently, our contention that the clusters with significant [Fe/H] variations are the remnant central star clusters of accreted dwarf galaxies is quite consistent with the Lee et al. (2007) results.

We end with one further point and that is an estimate of how many former dwarf galaxy nuclear star clusters, now seen as globular clusters with significant iron abundance intrinsic spreads, might be expected in the halo of the Milky Way, given that in our speculation four additional candidates beyond M54 and ω Cen are already identified. If we assume that the absolute visual magnitude of the Galactic halo is $M_V \approx -17$ (Freeman 1993) and that of order 50% of this luminosity is generated from the disruption of satellite galaxies with the remainder formed in-situ (e.g., Ivezić et al. 2012), and that the dominant contributors to the disrupted satellite population have typical luminosities comparable to the Fornax and Sagittarius dwarfs (i.e., $M_V \approx -14$ (McConnachie 2012)), then the disruption of only ~ 15 or so such systems is implied. Given that we do not expect all dwarfs of this luminosity to have nuclear star clusters, it is clear that for our speculation to be valid there should not be

more than a few additional Galactic globular clusters with significant intrinsic iron abundance spreads awaiting discovery. Harris (1996) lists 36 clusters with $M_V \leq -8$; of these 12 are included in Fig. 14. Of the remainder, some are “standard clusters” such as M92 and M3 for which there is no evidence for the presence of significant intrinsic iron abundance spreads. Nevertheless, there does remain a number of relatively unstudied clusters in this group. We predict future work will reveal the presence of intrinsic [Fe/H] spreads in a handful of these systems at most, else our speculation will have to be revisited.

In summary, we have used Ca II triplet spectroscopy of a large and well-defined sample of RGB members to establish that the luminous outer-halo globular cluster NGC 5824 possesses an intrinsic [Fe/H] dispersion. The dispersion is characterised by an inter-quartile range of 0.10 dex and a total abundance range of ~ 0.3 dex. NGC 5824 thus joins a small number of other Galactic globular clusters with intrinsic [Fe/H] abundance dispersions. As for ω Cen and M22, the abundance distribution rises steeply on the metal-poor side. The cluster is also apparently contained within an extended stellar envelope of $\lesssim 1$ kpc in size. Together these properties suggest that NGC 5824 may be the remnant nuclear star cluster of a former dwarf galaxy accreted and disrupted by the Milky Way.

ACKNOWLEDGEMENTS

G. Da C. would like to acknowledge research support from the Australian Research Council through Discovery Grant programs DP120101237 and DP120100475. He is also grateful for the support received during an extended visit to the Institute of Astronomy, University of Cambridge, and for shorter visits to Osservatorio Astronomico di Padova, INAF and ESO-Santiago.

Based in part on observations for program GS-2011A-Q-47 obtained at the Gemini Observatory, which is operated by the Association of Universities for Research in Astronomy, Inc., under a cooperative agreement with the NSF on behalf of the Gemini partnership: the National Science Foundation (United States), the Science and Technology Facilities Council (United Kingdom), the National Research Council (Canada), CONICYT (Chile), the Australian Research Council (Australia), Ministério da Ciência, Tecnologia e Inovação (Brazil) and Ministerio de Ciencia, Tecnología e Innovación Productiva (Argentina).

Based also in part on observations obtained under ESO program 087.D-0465.

REFERENCES

- Appenzeller, I., Fricke, K., Fürting, W., et al., *The Messenger*, 94, 1
- Battaglia, G., & Starkenburg, E. 2012, *A&A*, 539, A123
- Bekki, K., & Freeman, K. C. 2003, *MNRAS*, 346, L11
- Bekki, K., & Yong, D. 2012, *MNRAS*, 419, 2063
- Brocato, E., Buonanno, R., Malakhova, Y., & Piersimoni, A. M. 1996, *A&A*, 311, 778
- Carballo-Bello, J. A., Gieles, M., Sollima, A., et al. 2012, *MNRAS*, 419, 14
- Carretta, E., Bragaglia, A., Gratton, R., D’Orazi, V., & Lucatello, S. 2009, *A&A*, 508, 695
- Carretta, E., Bragaglia, A., Gratton, R. G., et al. 2010a, *A&A*, 520, A95
- Carretta, E., Bragaglia, A., Gratton, R. G., et al. 2010b, *ApJ*, 712, L21
- Carretta, E., Lucatello, S., Gratton, R. G., Bragaglia, A., & D’Orazi, V. 2011, *A&A*, 533, A69
- Carretta, E., D’Orazi, V., Gratton, R. G., & Lucatello, S. 2012, *A&A*, 543, A117
- Casetti-Dinescu, D. I., Girard, T., Herrera, D., van Altena, W. F., López, C. E., & Castillo, D. J. 2007, *AJ*, 134, 195
- Clement, C., Muzzin, A., Dufton, Q., et al. 2001, *AJ*, 122, 2587
- Cohen, J. G., Kirby, E. N., Simon, J. D., & Geha, M. 2010, *ApJ*, 725, 288
- Da Costa, G. S., Held, E. V., Saviane, I., & Gullieuszik, M. 2009, *ApJ*, 705, 1481
- Da Costa, G. S., & Marino, A. F. 2011, *PASA*, 28, 28
- D’Antona, F., Bellazzini, M., Caloi, V., Fusi-Peccì, F., Galilei, S., & Rood, R. T. 2005, *ApJ*, 631, 868
- Dinescu, D. I., Girard, T. M., & van Altena, W. F. 1999, *AJ*, 117, 1792
- Dotter, A., Chaboyer, B., Jevremović, D., Kostov, V., Baron, E., & Ferguson, J. W. 2008, *ApJS*, 178, 89
- Dubath, P., Meylan, G., & Mayor, M. 1997, *A&A*, 324, 505
- Harris, W. E. 1996, *AJ*, 112, 1487
- Ferraro, F. R., Dalessandro, E., Mucciarelli, A., et al. 2009, *Nature*, 463, 483
- Freeman, K. C. 1993, in *ASP Conf. Ser. 48, The Globular Cluster – Galaxy Connection*, ed. G. H. Smith & J. P. Brodie (San Francisco, CA: ASP), 608
- Gratton, R. G., Carretta, E., & Bragaglia, A. 2012, *A&A Rev.*, 20, 50
- Grillmair, C. J., Freeman, K. C., Irwin, M., & Quinn, P. J. 1995, *AJ*, 109, 2553
- Ivezić, Z., Beers, T. C., & Jurić, M. 2012, *ARA&A*, 50, 251
- Izzo, C., & Larsen, J. M. 2008, *FORS Pipeline User Manual, VLT-MAN-ESO-19500-4106, Issue 2.0, ESO Garching, 2008-09-09*
- Johnson, C. I., & Pilachowski, C. A. 2010, *ApJ*, 722, 1373
- Keeping, E. S. 1995, *Introduction to Statistical Inference*, 3rd edition (New York, NY: Dover)
- Koposov, S. E., Belokurov, V., Evans, N. W., et al. 2012, *ApJ*, 750, 80
- Lee, Y.-W., Gim, H. B., & Casetti-Dinescu, D. I. 2007, *ApJ*, 661, L49
- Majewski, S. R., Nidever, D. L., Smith, V. V., et al. 2012, *ApJ*, 747, L37
- Marcolini, A., Sollima, A., D’Ercole, A., Gibson, B. K., & Ferraro, F. R. 2007, *MNRAS*, 382, 443
- Marino, A. F., Milone, A. P., Piotto, G., et al. 2009, *A&A*, 505, 1099
- Marino, A. F., Sneden, C., Kraft, R. P., et al. 2011, *A&A*, 532, A8
- Marino, A. F., Milone, A. P., Piotto, G., et al. 2012, *ApJ*, 746, 14
- Martin, N. F., de Jong, J. T. A., & Rix, H.-W. 2008, *ApJ*, 684, 1075
- McConnachie, A. 2012, *AJ*, 144, 4
- Milone, A. P., Bedin, L. R., Piotto, G., et al. 2008, *ApJ*, 673, 241

- Mucciarelli, A., Bellazzini, M., Ibata, R., et al. 2012, MNRAS, 426, 2889
- Muñoz, C., Geisler, D., & Villanova, S. 2013, MNRAS, 433, 2006
- Newberg, H. J., Yanny, B., & Willett, B. A. 2009, ApJ, 700, L61
- Norris, J. E., Wyse, R. F. G., Gilmore, G., et al. 2010, ApJ, 723, 1632
- Origlia, L., Rich, R. M., Ferraro, F. R. 2011, ApJ, 726, L20
- Olszewski, E. W., Saha, A., Knezek, P., et al. 2009, AJ, 138, 1570
- Piotto, G., King, I. R., Djorgovski, S. G., et al. 2002, A&A 391, 945
- Rodgers, A. W., & Paltoglou, G. 1984, ApJ, 283, L5
- Roederer, I. U., Marino, A. F., & Sneden, C. 2011, ApJ, 742, 37
- Romano, D., Matteucci, F., Tosi, M., et al. 2007, MNRAS, 376, 405
- Romano, D., Tosi, M., Cignoni, M., et al. 2010, MNRAS, 401, 2490
- Sandage, A. 2006, AJ, 131, 1750
- Sarajedini, A., & Layden, A. C. 1995, AJ, 109, 1086
- Saviane, I., Da Costa, G. S., Held, E. V., et al. 2012, A&A, 540, A27
- Simmerer, J., Ivans, I. I., Filler, D., Francois, P., Charbonnel, C., Monier, R., & Gaël, J. 2013, ApJ, 764, L7
- Sobeck, J. S., Kraft, R. P., Sneden, C., et al. 2011, AJ, 141, 175
- Sollima, A., Gratton, R. G., Carballo-Bello, J. A., et al. 2012, MNRAS, 426, 1137
- Wylie-de Boer, E., Freeman, K. C., & Williams, M. 2010, AJ, 139, 636
- Yong, D., Grundahl, F., D'Antona, F., et al. 2009, ApJ, 695, L62
- Yong, D., Meléndez, J., Grundahl, F., et al. 2013, MNRAS, 434, 3542